The chemical shifts of Xe in the cages of clathrate hydrate Structures I and II

Dirk Stueber and Cynthia J. Jameson[a)]
Department of Chemistry, M/C-111, University of Illinois at Chicago, Chicago, Illinois 60607-7061

(Received 28 August 2003; accepted 20 October 2003)

We report, for the first time, a calculation of the isotropic NMR chemical shift of ^{129}Xe in the cages of clathrate hydrates Structures I and II. We generate a shielding surface for Xe in the clathrate cages by quantum mechanical calculations. Subsequently this shielding surface is employed in canonical Monte Carlo simulations to find the average isotropic Xe shielding values in the various cages. For the two types of cages in clathrate hydrate Structure I, we find the intermolecular shielding values $[\sigma(\mathrm{Xe@}5^{12}\,\mathrm{cage})-\sigma(\mathrm{Xe\,atom})]=-214.0$ ppm, and $[\sigma(\mathrm{Xe@}5^{12}6^{2}\,\mathrm{cage})-\sigma(\mathrm{Xe\,atom})]=-146.9$ ppm, in reasonable agreement with the values -242 and -152 ppm, respectively, observed experimentally by Ripmeester and co-workers between 263 and 293 K. For the 5^{12} and $5^{12}6^{4}$ cages of Structure II we find $[\sigma(\mathrm{Xe@}5^{12}\,\mathrm{cage})-\sigma(\mathrm{Xe\,atom})]=-206.7$ ppm, and $[\sigma(\mathrm{Xe@}5^{12}6^{4}\,\mathrm{cage})-\sigma(\mathrm{Xe\,atom})]=-104.7$ ppm, also in reasonable agreement with the values -225 and -80 ppm, respectively, measured in a Xe-propane type II mixed clathrate hydrate at 77 and 220–240 K by Ripmeester *et al.* © *2004 American Institute of Physics.*
[DOI: 10.1063/1.1632895]

INTRODUCTION

The applications of ^{129}Xe NMR spectroscopy, in particular, the use of hyperpolarized ^{129}Xe, as a probe for the electronic environment and structure of nanocavities and nanochannels in inorganic materials, organic molecular crystals, polymers, proteins, and biosensors,[1–10] take advantage of the exquisite sensitivity of the chemical shift of the Xe atom to the electronic structure and the spatial arrangement and distribution of the atoms that it encounters in these confining structures. The unique advantage of employing the Xe atom as a probe is that intermolecular interactions directly affect the electronic environment of the observed nucleus. Whereas the isolated Xe atom has a purely diamagnetic nuclear magnetic shielding, any deviation from spherical symmetry brought about by intermolecular interactions necessarily creates paramagnetic shielding contributions that deshield the Xe nucleus relative to the free atom. The latter is the commonly used reference state for specifying the shielding differences that are experimentally measured as ^{129}Xe NMR chemical shifts.[11]

In the presence of another rare gas atom, the Xe atom experiences a deshielding that depends on the distance from the neighbor and the electronic structure of the neighbor and also the orientation of the Xe–Rg axis in the applied magnetic field. Therein originates the ability of the ^{129}Xe nucleus in the Xe atom to discriminate between different environments. For example, at a given distance, say 3.5 Å, when the neighbor is another Xe atom, the isotropic deshielding is very pronounced, -195.7 ppm, and diminishing in the series Kr, Ar, and Ne, respectively, -87.5, -44.8, -5.5 ppm relative to the isolated Xe atom.[12] For a given neighbor, the dependence of the Xe shielding response on the distance is also very pronounced. For example, the Xe deshielding is -493.2, -66.6, -6.8 ppm, respectively, interacting with another Xe atom at 3.0, 4.0, and 5.0 Å.[12] (We have used shielding values calculated at the Hartree–Fock level for an illustration here.) These two factors, the greater Xe deshielding with shorter distances and the greater deshielding in the presence of neighbors with ''more available'' electrons, together permit the Xe shielding response to discriminate between environments. Thus, the Xe shielding response is unique to a particular arrangement of particular types of atoms, i.e., the configuration of its neighbors. At the same time, the probability of finding Xe in a particular configuration of surrounding atoms determines how much each shielding response can contribute to the overall average shielding. Thus, every observed ^{129}Xe average chemical shift relative to the isolated Xe atom is a convolution of two mathematical hypersurfaces: the shielding response surface and the potential energy surface; both are functions of coordinates. After constructing the shielding surface from quantum mechanical calculations, and the potential surface from multiproperty analyses, we have found that it is possible to use Monte Carlo grand canonical simulations to calculate the average ^{129}Xe NMR chemical shifts in aluminosilicate and aluminophosphate cages and channels. In particular, we obtained average ^{129}Xe chemical shifts in the cages of zeolite type A, with pure xenon gas[13,14] and with mixtures of sorbates,[15–17] and in the channels of silicalite (zeolite ZSM-5),[18] and ALPO-11,[19] as a function of loading and composition. Furthermore, by adopting a dimer tensor model, we have found that it is possible to predict in general the NMR lineshapes that one might expect to observe for an average shielding tensor of Xe at various occupancies in nanochannels of these materials.[19,20] We also have made some progress in calculating lineshapes for ^{129}Xe in channels containing aromatic

a)Electronic mail: cjj@sigma.chem.uic.edu

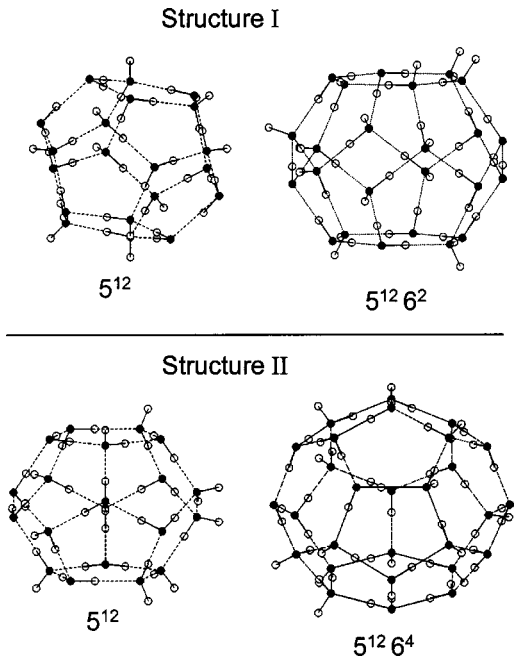

FIG. 1. The structure of the four cages in clathrate hydrate Structures I and II, based on the diffraction data of Refs. 31 and 32. The filled circles represent oxygen atoms and the open circles hydrogen atoms of the water molecules that comprise the cages.

rings in molecular crystals, and for ^{129}Xe in organic cages.[21]

That the intermolecular shielding response falls off greatly with increasing distance is fortunate from a theoretical point of view in that one only needs to include immediate neighbors in considering the Xe environment. However, this is misleading if interpreted to mean that the atoms at larger distances away from the Xe atom play no role in the shielding response. In this paper, we consider examples in which it becomes important to consider a sizable crystal fragment in order to obtain a reasonably realistic description of the Xe shielding response. When the atoms that are the immediate neighbors of the Xe atom are participants in an extended hydrogen-bonding network that extends throughout an entire crystal, the molecules that are the nearest neighbors of the Xe atom are, by themselves, insufficient to describe the environment experienced by the Xe atom. We treat two examples of such systems, the clathrate hydrates Structures I and II. In clathrate hydrate Structure I, the water molecules constitute two types of cages in which the Xe atom may be trapped: the smaller more symmetrical 5^{12} cage, with 12 pentagonal faces and the more disklike, somewhat larger $5^{12}6^2$ cage having two additional hexagonal faces. Clathrate hydrate Structure II also forms two types of cages: 5^{12} and $5^{12}6^4$. These four types of cages are shown in Fig. 1. The body of excellent experimental work on Xe in clathrates has been done nearly entirely in the laboratory of J. A. Ripmeester and his co-workers.[22–27] More recently, since the availability of hyperpolarized ^{129}Xe technology, other groups have begun to study ^{129}Xe in clathrate hydrates as well.[28] The isotropic ^{129}Xe chemical shifts that we wish to understand quantitatively arise from early work in the Ripmeester laboratory.[22–24] Although more recent results with hyperpolarized ^{129}Xe have been reported by the group,[29,30] the early chemical shift values have not been superceded. In this work we will focus entirely on the simulation of the isotropic ^{129}Xe chemical shifts and the general approach that allows for a realistic description of the disordered hydrogen-bonded network to provide for a reasonably good description of the Xe environment in the clathrate hydrate cages. The lineshapes and the ^{131}Xe nuclear quadrupole coupling will be considered later.

There are several goals of this study besides attempting to reproduce the observed ^{129}Xe isotropic shifts in the small and large cages of clathrate hydrates. In the process of doing the calculations, we expect to shed light on some more general questions concerning the effects of long-range interactions and hydrogen bonding on Xe nuclear magnetic shielding.

(a) We expect to determine the shielding at the nucleus of a Xe atom located at the position that corresponds to the center of the small cage (also the large cage) in the presence of only point charges that represent the infinite clathrate hydrate crystal lattice, with no oxygen or hydrogen atoms (i.e., no electrons). This would show the shielding due to the effect of electrical polarization of the Xe atom alone. We expect this to be small, although others have assumed electrostatic contributions to shielding as a primary mechanism for intermolecular effects on chemical shifts. The goal is to show it is indeed small for Xe, as we have predicted.

(b) We expect to determine the shielding at the nucleus of a Xe atom located at the center of an isolated cage carved out of the lattice, in other words, including only the water molecules of the cage itself in the shielding calculations, omitting the rest of the crystal. The long-range influence of the rest of the crystal on the electrons of the Xe atom and the long-range effects on the water molecules of the cage are not included.

(c) We expect to determine the shielding at the nucleus of a Xe atom located at the center of a cage of water molecules embedded inside an array of point charges that simulates the electrostatic effects of the rest of the crystal.

(d) We also consider a model that takes into account the full hydrogen bonding (not only the electrostatic part of the hydrogen bonding) of the cage water molecules. For this we need to represent the cage water molecules as well as at least the first shell of water molecules that provide the full complement of hydrogen-bonding partners of the cage waters.

(e) Finally, we consider a model that provides fully the hydrogen-bonding partners to the cage containing the Xe atom, as in the model above, and in which the water molecules in the rest of the crystal lattice are represented by point charges.

We want to compare (a)–(e) and thereby determine the following: to what extent is the observed shielding at the Xe nucleus due to (i) the long-range point charges directly, (ii) the electrons of the water molecules of the cage only, (iii) the influence of the long-range point charges on the electronic structure of the water molecules of the cage, and the conse-

quence of this to the shielding of Xe, (iv) the influence of the covalent part of the hydrogen bonding on the ability of the cage waters to provide the appropriate electronic response to the Xe atom that generates the shielding response at the nucleus.

METHODS

The representation of the clathrate hydrate structure

The neutron diffraction studies of a Xe Structure I clathrate hydrate[31] and a mixed Xe/CCl_4 Structure II clathrate hydrate[32] provide the positions of the oxygen and hydrogen atoms, however, the hydrogen positions possess only half occupancy. The remaining proton disorder in clathrate hydrates even at 0 K, leads to the residual entropy in ice.[33] The ''ice rules'' state that[34] (1) ice consists of intact water molecules. (2) The oxygen atoms form a lattice with tetrahedral coordination. (3) The bond between two neighboring oxygen atoms can accommodate one and only one proton belonging explicitly to one of the two oxygens. (4) All proton configurations satisfying the above three conditions are equally probable.

Starting from neutron diffraction data, implementing the ice rules means satisfying the two constraints: (1) only one of the two positions between two oxygen nuclei can be occupied by a hydrogen atom, and (2) each oxygen atom must have exactly two hydrogen atoms at covalent O–H distances and exactly two hydrogen atoms at O–H hydrogen-bonding distances. Naturally, in our shielding simulations we have to use a clathrate hydrate structure that complies with the ice rules. In order to generate a valid hydrogen configuration, we start out by placing only one hydrogen atom at one of the two possible positions in the line between two oxygen atoms. This guarantees that we have the correct stoichiometry and that we also satisfy the first constraint. This results in an incorrect initial configuration in which oxygens can have zero to four covalent bonds. In order to satisfy constraint 2 without violating constraint 1, we rearrange the hydrogen atoms in such a way that we only shift hydrogens along the O—O line and not off the line onto another O—O line. The shifting of one hydrogen atom back and forth between the two known positions along each O—O line is carried out using a Monte Carlo procedure, with a penalty associated to any shift that corresponds to an increase in the number of violations of the ice rules. The random shifting is performed until the deviations from the ice rules is down to a number low enough that random shifting becomes inefficient. The next step is specifically targeting the ''problem'' oxygen atoms, those oxygens with greater or fewer than two covalently bonded hydrogens. The idea is to generate chains of H shifts that propagate through the simulation box, starting from one problem oxygen toward another. An allowed chain step decreases or retains the total number of deviations; no uphill steps are allowed. If a chain is terminated, a new problem oxygen is chosen and a new chain is started from that oxygen. A successful chain termination occurs when the chain connects two problem oxygens, resulting in a configuration in which both oxygens possess two covalently bonded hydrogen atoms. A chain is abandoned when it encounters an oxygen or hydrogen atom already used in a previous or the current chain, or else encounters the periodic image of one of the points already on the chain (to prevent the chains from running in loops), or when none of the possible hydrogen shifts result in a decrease of deviations. This chain propagation method proved to be very efficient for generating relatively large simulation boxes (supercells) with proton configurations that completely comply with the ice rules under periodic boundary conditions. Figure 2 shows as an example the number of deviations from the ice rules as a function of proton switching steps for generating a valid proton configuration for a Structure I clathrate hydrate supercell containing 2944 water molecules ($4\times4\times4$ crystallographic unit cells). It is apparent from the plot that random switching is very efficient in the beginning, quickly reducing the number of deviations from the ice rules, however, becomes essentially useless at a certain point in the process. At this point, the chain propagation method very effectively reduces the remaining deviations to zero, yielding a supercell with a valid proton configuration under periodic boundary conditions.

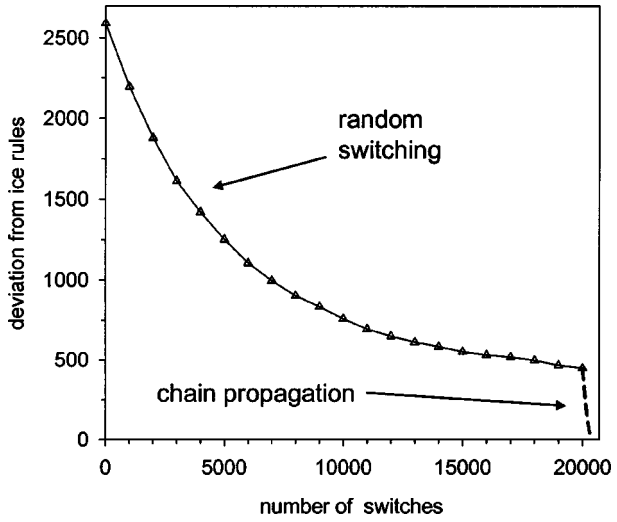

FIG. 2. The comparative efficiency of random shifting (first stage) and chain propagation (last stage) in achieving a proton configuration that obeys the ice rules in 2944 water molecules of clathrate hydrate Structure I under periodic boundary conditions. Note the much faster convergence to the desired zero deviation configuration at the last stage.

The models

To investigate the contributions of long-range effects and hydrogen bonding on the shielding response at the Xe nucleus, we carried out quantum mechanical shielding calculations in five model systems with a type I clathrate hydrate structure.

(1) CAGE: This model includes only the Xe atom and the 20 water molecules in the 5^{12} cage or the 24 molecules in the $5^{12}6^2$ cage.
(2) XCAGE: This model includes the Xe atom, the water molecules that constitute the cage and all the water molecules that are required in order to provide the hydrogen-bonding partners of every water molecule in the cage. We refer to the cage together with its first coordination

shell as the extended cage. For the 5^{12} cage the extended cage consists of a total of 40 water molecules. For the $5^{12}6^2$ cage the extended cage consists of 48 water molecules.

(3) PCA: This model includes only the Xe atom. All water molecules in the crystal fragment are represented by point charges.
(4) CAGE/PCA: This model includes the Xe atom, the water molecules of the cage just as in the CAGE model, with the addition that the remaining water molecules in the crystal fragment are represented by point charges.
(5) XCAGE/PCA: This model consists of the Xe atom, the extended cage, and an array of point charges that represents the remaining water molecules in the crystal fragment.

To construct each of the five models, we started out by generating a valid proton configuration (configuration A) for one crystallographic unit cell using the random shifting and chain propagation procedure outlined above. Subsequently, this unit cell was replicated to form a crystal fragment of $4\times4\times4$ unit cells in size (2944 water molecules). The coordinates of the entire fragment were translated so that its center (the origin of the coordinate system) coincided with the center of the cage under investigation (5^{12} or $5^{12}6^2$). The crystallographic coordinates of the fragment provides the coordinates of the oxygen and hydrogen atoms, as well as the coordinates for the point charges utilized in the models. The actual point charge values used in these models to simulate the electrostatic effects of the infinite crystal lattice are obtained by employing the Embedded Ion Method that has been described earlier by one of us.[35] This method simulates the electrostatic crystal potential that is experienced by a given atom inside an infinite crystal lattice, the Madelung potential, with a finite, self-consistent array of point charges. This point charge array is generated in a fitting procedure using the Ewald summation method. By adjusting the size of the array and of particular zones within the array, the potential that is produced by the array at a defined central region, the Ewald potential, may be tuned to the Madelung potential with a certain accuracy. The actual computational process conducted in the EIM utilizes the potential produced by the finite point charge arrays in conjunction with the quantum mechanics suite of programs, GAUSSIAN,[36] to obtain the shieldings of interest. In the first part of the EIM, a self-consistent point charge array is obtained in an iteration procedure between the EWALD program and GAUSSIAN. Subsequently, the shieldings of interest are calculated for a given atom embedded inside the point charge array, located inside its central region, using GAUSSIAN. In the models used in the present study, the zones in which the Madelung potential is reproduced in the Ewald calculations were made large enough to contain the Xe atom and the water molecules of the extended cages under investigation.

In order to investigate the effects of the proton disorder in clathrate hydrate crystals on the Xe shielding, two additional versions of the XCAGE/PCA model for the small cage were generated, each one based on a different proton disorder (configurations B and C) of the starting unit cell. The five models are illustrated in Fig. 3.

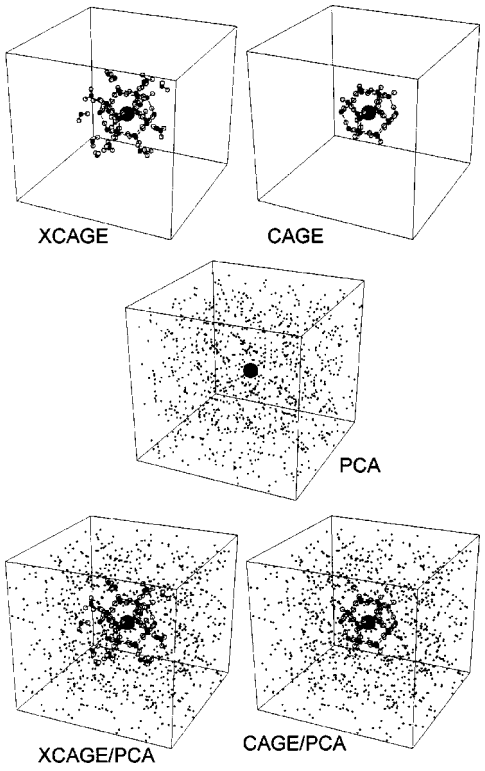

FIG. 3. Model systems used in the *ab initio* and DFT calculations of Xe shielding in the 5^{12} cage of clathrate hydrate Structure I. Atoms represented with all electrons are shown as balls. Atoms represented by point charges are drawn as dots.

Ab initio and DFT shielding calculations

For the quantum mechanical calculations of Xe shielding, we use gauge-including atomic orbitals (GIAO) that have been shown to provide an advantage when used with any size of basis set, but especially for modest-sized ones, since they provide the correct first-order wave functions for an atom in the presence of an external magnetic field.[37] We used both Hartree–Fock (HF) and density functional (DFT) methods. We employ 240 basis functions for Xe, as described in our previous work, starting from the compilation of Partridge and Faegri[38] and augmented with polarization functions according to the recipe by Bishop *et al.*[39] This basis set was specifically constituted to describe the shielding response of Xe under the influence of a static electric field. It is so well balanced for this purpose that we have found full counterpoise corrections,[40] even with 1200 additional basis functions on the neighboring atoms, amount to mere hundredths of a ppm at the typical distances of interaction. For the water molecules we used a D95** basis set, which is a Dunning–Huzinaga full double zeta basis set augmented with three sets of p and one set of d polarization functions.[41] All shielding calculations were carried out utilizing the GAUSSIAN package,[36] using coordinates derived from the neutron-diffraction data.[31,32] The lattice parameter appropriate to 275 K was chosen for the clathrate structure, based on the diffraction data of Ikeda *et al.* for Structure I.[31] To

answer the questions (a)–(e) posed in the Introduction, shielding calculations were carried out for Xe in the center of the small and large cages for each of the five models described above.

The Xe shielding function in a clathrate hydrate

A single-point quantum mechanical shielding calculation for a Xe atom located at the center of a clathrate cage does not provide a complete description. It is anticipated that a proper comparison with the experimentally observed ^{129}Xe chemical shift values will require permitting the Xe to explore an arbitrarily large number of positions within the cage, especially for a large cage. Positions close to the atoms of the cage at which the Xe has a small but not negligible probability of being found at the temperature of the experiment have to be included because the shielding function is known from our previous work to be significantly more deshielding at closer contact. These calculations are carried out using the most realistic model, the XCAGE/PCA.

Our general approach for constructing shielding surfaces is to calculate quantum mechanically the shielding values for various nuclear configurations and then to describe the collection of shielding values with a mathematical function of coordinates for the given configuration. In this particular application, Xe shielding values are calculated at various positions along trajectories that approach the cage walls from the center of the cage. The positions are chosen to sample many different molecular environments that the Xe atom can experience within the cages. Subsequently the shielding values are fitted to the following general form:

$$\sigma(\mathrm{Xe},\mathbf{r})-\sigma(\text{free Xe atom}) = \sum_i a_6 r_{\mathrm{XeOi}}^{-6} + a_8 r_{\mathrm{XeOi}}^{-8} + a_{10} r_{\mathrm{XeOi}}^{-10} + a_{12} r_{\mathrm{XeOi}}^{-12} + \sum_k b_6 r_{\mathrm{XeHk}}^{-6} + b_8 r_{\mathrm{XeHk}}^{-8} + b_{10} r_{\mathrm{XeHk}}^{-10} + b_{12} r_{\mathrm{XeHk}}^{-12}. \quad (1)$$

In other words, it is assumed that the *ab initio* or DFT result can be described in terms of sums over the shielding response contributions from the Xe–O interactions and contributions from the Xe–H interactions, each of which is merely a function of distance (a shielding function). The form of the distance dependence used in Eq. (1) has been found to be completely adequate in describing the Xe *ab initio* and also the DFT shielding values for Xe–Xe, Xe–Kr, Xe–Ar, and Xe–Ne at a large number of separations.[12] The fit is constrained such that the Xe–O and Xe–H shielding functions individually correctly approach zero at large distances. We will demonstrate how well this description fits the Xe shielding values obtained for Xe in the cages of the clathrate hydrates studied here. Note that we only use the function as a description of the actual *ab initio* values. It is not incorrect to think of it as a rather intelligent interpolating function because the functional form is based on the *ab initio* results for Xe with only one neighbor atom.

Investigation of the effect of the local proton disorder

The disordered proton configuration of the specific cage in which the Xe shielding calculation is carried out poses a problem. Ideally, a molecular dynamics (MD) simulation, in which the water molecules are allowed to change orientations, should be performed. This requires a sophisticated force field including many-body terms that account for hydrogen bonding interactions accurately and able to reproduce the crystallographic clathrate hydrate structure. An average over many quantum mechanical calculations of the Xe shielding carried out every few MD steps accumulated over a long simulation time would then provide the average Xe shielding. This approach is not practically feasible. The static equivalent of this procedure is to perform shielding calculations in static cages, each with a specific proton configuration, provided that we sample a sufficient number of local environments for the Xe. Following the latter approach, we started out with three different proton configurations (configurations A, B, and C) for the 5^{12} cage, and one (configuration A) for the $5^{12}6^2$ cage in clathrate hydrate Structure I. The shielding calculations were carried out, using the XCAGE/PCA model, at 16 positions in the small cage for each of the proton configurations A, B, and C, and 25 positions in the large cage for proton configuration A.

In order to verify that we have done *ab initio* calculations in a sufficient number of proton configurations to represent the general Xe shielding function in a clathrate hydrate, we investigated the proton distribution functions for each of the XCAGE/PCA models used for *ab initio* shielding function calculations in both the small 5^{12} cage and the larger $5^{12}6^2$ cage. Since the oxygen atoms are in the same positions and only the proton positions vary, a useful indicator for comparing similarities and differences of proton configurations is the distribution of distances from the center of the cage, where the Xe has the highest probability of being found. Thus, we determined distributions of proton distances (fraction of protons at each distance) from the center of the cage (a) for each individual XCAGE/PCA used (configurations A, B, and C), (b) for three 5^{12} cage models (A, B, and C) taken together, and (c) for the supercell containing 2944 water molecules. All were compared with the proton distance distribution of the crystallographic average structure, which has a 1/2 population at each proton position.

Monte Carlo simulations

Averaging of the Xe shielding is carried out using canonical Monte Carlo simulations. The disadvantage of this approach is that we will be unable to consider the effects on the shielding of a given Xe atom arising from the distributions of Xe atoms in neighboring cages. This does not appear to be important for Xe shielding in low occupancy clathrates, although Ripmeester *et al.* have demonstrated that the occupancy of the adjoining cage in some clathrates can have a measurable effect on the ^{129}Xe chemical shift.[42] Since the Xe–Xe intermolecular shielding is negligible at distances greater than 6 Å, and in any case, we usually use a cut-and-shifted Xe–Xe shielding function that is zero at r_{XeXe}

TABLE I. Potential parameters used in this work, $V=\epsilon\{[6/(n-6)]\check{r}^{-n}-[n/(n-6)]\check{r}^{-6}\}$, where $\check{r}=r/r_{\min}$, $n=m+\gamma(\check{r}-1)$.

	m	γ	$r_{\min}$, Å	ϵ/k_B, K
Xe–O	13	5	3.724	105.42
Xe–H	13	9.5	3.471	73.07

$\geqslant$6.5 Å, the Xe–Xe contributions to the calculated average shielding will be neglected. Pairwise additive potentials of the Maitland–Smith form[43] were used,

$$V=\epsilon\{(6/n-6)\check{r}^{-n}-(n/n-6)\check{r}^{-6}\},$$

where n is allowed to vary with $\check{r}=r/r_{\min}$ according to $n=m+\gamma(\check{r}-1)$. For the Xe–O potential we start with the Xe–Ne parameters, namely $m=13$, $\gamma=5$, $\epsilon/k=65.42$ K, $r_{\min}=3.924$ Å.[43] For the Xe–H potential we start with the parameters based on agreement with molecular beam scattering and other properties for Xe–CH_4 ($m=13$, $\gamma=9.5$, $\epsilon/k=53.07$ K, $r_{\min}=3.671$ Å).[17] In both cases we increased the well depth and decreased the $r_{\min}$ to the final set of Xe–O and Xe–H parameters given in Table I. The simulation box is a supercell under periodic boundary conditions.

We do not explicitly include induction terms in our potential; no charges are involved in the Monte Carlo averaging of the Xe shielding. All atoms in the simulation box and their periodic images are treated as atoms in the Monte Carlo canonical averaging. Since the Xe–O and Xe–H shielding functions correctly approach zero at large distances, a cut-and-shifted shielding function can be used in parallel with a cut-and-shifted potential function, although the cut distances are not required to be identical.[13,44] Most of the atoms beyond the first shell of waters hydrogen bonded to the water molecules of the cage containing the Xe atom lie at distances greater than the shielding cutoff distance.

The supercell has to be sufficiently large to include a representative number of proton configurations for the individual cages containing Xe and small enough for efficiency. We investigated the optimum size of the representative supercell for the Monte Carlo simulations of Structure I by using simulation boxes consisting of 1 unit cell, 2×2×2, 4×4×4, and 6×6×6 unit cells. In each case the crystal fragment with $n\times n\times n$ unit cells was constructed from the neutron diffraction coordinates,[31,32] a valid proton disorder was generated for the entire fragment, utilizing random shifting followed by the chain propagation method, as described above. We find that the optimum size of the simulation box is 4×4×4 for Structure I. The comparable size for Structure II is 2×2×2 unit cells. Both are large enough so that a Xe atom will be placed in cages with diverse proton arrangements. Final averaging of the Xe shielding was carried out in these supercells containing, respectively, 2944 and 8704 water molecules for Structures I and II.

Finally, average isotropic shieldings for Xe were obtained in four separate Monte Carlo simulations in which single Xe atoms populate only those cages of a particular type: 5^{12} or $5^{12}6^2$ in Structure I, 5^{12} or $5^{12}6^4$ in Structure II. For each simulation, initially, a Xe atom was placed at the center of each of the respective cages within the supercell. After a large number of Metropolis-weighted displacement moves, the average isotropic shielding is obtained. The final averages reported here correspond to 1 280 000 Xe configurations for all cage types, except for $5^{12}6^4$ in Structure II, where we used 3 840 000 Xe configurations. The temperature chosen for the simulations is 275 K, the same temperature as the earliest reported experimental spectra of Xe in clathrate hydrates.[22,23]

TABLE II. Single-point calculations; isotropic shielding of Xe at the center of the 5^{12} cage in Structure I, $\sigma_{iso}-\sigma$(Xe atom), ppm.

Model	PCA	CAGE	XCAGE	CAGE/PCA	XCAGE/PCA
HF	−0.4	−142.1	−138.2	−114.0	−119.4
B3LYP	−0.5	−226.6	−217.0	−184.9	−199.4

RESULTS AND DISCUSSIONS

Single-point calculations; Xe shielding at the center of the cage

As an initial assessment of the various models, we employ the Xe isotropic shielding at the center of the two cages in Structure I. These results are shown in Tables II and III for each of the five models.

The isotropic shifts obtained in Hartree Fock and density functional theory calculations for a Xe atom located at the centers of the 5^{12} and $5^{12}6^2$ cages are given in Tables II and III, respectively. For every model system used in this work, the Hartree–Fock calculations uniformly provide a significantly smaller deshielding response at the Xe nucleus than the DFT/B3LYP method does. It has been previously noted that the shielding of the oxygen nucleus in the water molecule is inadequately represented at the HF level, as it is usually found for atoms bearing lone pairs.[45] Our results in Tables II and III show that the water molecules of the cage also give an incomplete shielding response to the Xe atom when electron correlation is not included. In other intermolecular Xe shielding calculations, for example, Xe interacting with rare gas atoms (Rg)[12] or with CO_2, CO, or N_2, we have found that DFT/B3LYP gives values that are more deshielded than the values obtained in HF calculations.[21] Where averaging can be highly accurate, as for Xe–Rg and Xe–CO_2, a comparison with gas phase experiments establishes that there are electron correlation contributions to the Xe intermolecular shielding (of the order of 15% in Xe–Rg pairs) that are not included in HF calculations.[12,21] On the other hand, the B3LYP values for these systems are too deshielding by about the same amount. In systems where electron correlation is important in the description of the neighboring molecules, the intermolecular Xe shielding values calculated using the HF method can be significantly in-

TABLE III. Results of single-point calculations of the isotropic shielding of Xe at the center of the $5^{12}6^2$ cage in Structure I, $\sigma_{iso}-\sigma$(Xe atom), ppm.

Model	PCA	CAGE	XCAGE	CAGE/PCA	XCAGE/PCA
HF	−0.2	−80.0	−75.5	−53.4	−59.3
B3LYP	−0.3	−138.1	−128.0	−100.8	−111.0

adequate, as we demonstrated in the $Xe@C_{60}$ example.[21] These findings indicate that the DFT/B3LYP method should be preferred over the HF method for calculating the Xe shielding response in clathrate hydrates, and for the remainder of this paper we discuss the results derived from DFT/B3LYP calculations exclusively.

Xe located at the center of the 5^{12} cage

The PCA model represents all the oxygen and hydrogen atoms in a crystal fragment by an array of partial charges with no electrons to invoke a Xe response, thus results in a very small deshielding effect at the Xe nucleus (−0.5 ppm, independent of the size of the point charge array that was used). It is clear that Xe shielding does not primarily arise from the polarization of its electrons by electrostatic charges, an incorrect but commonly suggested mechanism for its observed chemical shifts.

The CAGE model with every oxygen having truncated hydrogen bonds provides the largest deshielding response of all the models (−226.6 ppm).

The CAGE/PCA model provides a smaller deshielding response at the Xe nucleus (−184.9 ppm) than the CAGE model. This change in Xe shielding from the CAGE model to the CAGE/PCA model is brought about by the point charge array providing, to a limited extent, the hydrogen bonding that is missing from the isolated cage. Thus, the CAGE/PCA model provides a more accurate description of the Xe environment in the real clathrate crystal than the CAGE model. These three are standard models used in the initial applications of the EIM method.[35,46,47] The results obtained at this stage have made it apparent that we need to go beyond the standard approaches in order to generalize the EIM method for an application to extended networks of hydrogen-bonded systems.

Two major problems are revealed by the single-point calculations in the simpler models: (a) How do we take into account a better hydrogen-bonding description for the H_2O molecules that ''touch'' the Xe atom? (b) How do we average over the disorder of the protons? We discuss the latter in the next section.

We can attribute the change in shielding in going from the CAGE model to the CAGE/PCA model to a change in the distribution of electron density in the water molecules of the cage due to the point charges. The point charges do not compensate enough to replace fully the truncated hydrogen bonds in the CAGE/PCA model. One possible solution is to include the hydrogen-bonding partners of the cage molecules in the model so that the Xe atom is involved in short-range interactions with water molecules that have their full complement of hydrogen bonds. This can be achieved by creating a crystal fragment that contains the water molecules of the cage and the water molecules of the first surrounding shell of water molecules, so that the truncated hydrogen bonds are shifted to the surrounding shell. This is the XCAGE model.

The necessity for including a first coordination shell, especially in hydrogen-bonded systems is certainly well known for those cases where the nucleus of interest is itself taking part in the hydrogen-bonding network. See, for example, the calculations conducted by Peter Pulay and his co-workers on the proton shielding tensor in ice, which required the water molecule to be surrounded by its 16 immediate neighbors in order to produce a proton shielding anisotropy that agreed with experiment.[48] The calculations by Gang Wu on the ^{17}O shielding tensor in crystalline urea required seven urea molecules in order to obtain tensor components that agree reasonably well with the experimental values. Six urea molecules are hydrogen-bond donors (4) and acceptors (2) to the urea where the nuclear shielding is being investigated.[49]

It now appears that an accurate description of the Xe shielding response to hydrogen-bonded systems requires the inclusion of at least the first coordination shell of a given cage. Table II shows that the effects of having truncated hydrogen bonds at the oxygen atoms whose electrons have overlap and exchange with the Xe electrons are severe in the CAGE model but less pronounced in the XCAGE model. The XCAGE model results in a smaller deshielding for Xe than the CAGE model (−217.0 versus −226.6 ppm). This extended cage can then be placed in the point charge array that represents the rest of the infinite crystal; this is the XCAGE/PCA model. In this model, the point charge array provides the electrostatic part of the hydrogen bonding for the water molecules of the first coordination shell of the cage and should have a less dramatic effect on the Xe shielding response as compared to going from the CAGE to the CAGE/PCA model. We find that this is indeed the case, a drop of 17.6 ppm in going from the XCAGE model to the XCAGE/PCA model, compared to a drop of 41.7 ppm in going from the CAGE model to the CAGE/PCA model. The trends in the shielding values calculated for our model systems clearly indicate that the more shells of water molecules we include in the calculations, the closer we approach the real situation. However, including two shells of water molecules would require a substantially more demanding calculation since the number of water molecules increases significantly after the first shell.

Xe located at the center of the $5^{12}6^2$ cage

The results for the $5^{12}6^2$ cage shown in Table III reveal the same trends among the different models as those obtained for the small cage. However, the isotropic shift values at the Xe nucleus obtained for all models of the large cage are significantly lower than for the small cage (about 80 to 90 ppm for all but the PCA model), reflecting the longer distances of the cage atoms from the center of the cage. The trend is in agreement with experiment. The calculated chemical shift anisotropy (not shown) also reflects the disklike shape of the cage. The PCA model for the large cage results in a deshielding response barely smaller than for the small cage, but this is almost irrelevant since the PCA model in general produces a nearly negligible shielding response.

The Xe shielding values obtained at the center of the cage in the five model systems clearly reveal that including the full complement of hydrogen-bonding partners of the cage waters improves the description of the electronic structure of the cage that, in turn, generates a more accurate shielding response at the Xe nucleus. Including a point charge array that mimics the effect of the remaining infinite

crystal lattice is essentially as important to complete the electronic description. This leads to the conclusion that the XCAGE/PCA model represents the best compromise of accuracy and feasibility. From this point on, we abandon the simpler models and consider only the XCAGE/PCA model.

Accounting for proton disorder

In the crystal, two dynamic processes have been identified: the reorientation of water molecules at their lattice sites and center of mass diffusion. The water molecule reorientation process has been studied extensively for Structure I and Structure II hydrates.[50] Several different symmetry situations and motional regimes can be distinguished. When water molecular motions are rapid, the hydrate cages take on their true crystallographic symmetry on time average. In this instance (Xe in spherical cages 5^{12} in Structure I and the $5^{12}6^4$ in Structure II) the ^{129}Xe peak observed in the NMR spectrum is narrow and has an isotropic lineshape. In the case of the nonspherical cages ($5^{12}6^2$ in Structure I and 5^{12} in Structure II) the ^{129}Xe exhibits an anisotropic line shape.[24] At low temperatures, when the water molecules are static on the NMR time scale, the proton disorder is frozen in, and all cages will have a local symmetry (much lower than the space average crystallographic symmetry) that varies from cage to cage depending on proton configuration. The experimental ^{129}Xe chemical shifts we are comparing our results with were taken at 200–275 K when water molecular motions (reorientations, in particular) are rapid,[22,24] so the Xe finds itself in a site with true crystallographic symmetry on time average. On the other hand, in our model systems the Xe finds itself in a site with a fixed local proton disorder and, when using a small replicating unit (the unit cell), even the long-range proton order in the PCA model for the crystal fragment is lower than the space average crystallographic symmetry.

How do we determine the average Xe shielding that reflects an average equivalent to that which would have been obtained in hydrate cages with true crystallographic symmetry on time average, that is, without doing molecular dynamics and *ab initio* shielding calculations every few time steps? The static equivalent is to do Monte Carlo averaging in a crystal fragment that possesses the space average crystallographic symmetry. This is usually done by making large supercells and using these as the propagating unit with which to create the periodic infinite solid. See, for example, the series of papers by Mauri and co-workers on disordered systems such as amorphous materials[51] and hexagonal ice.[52] We can generate a large supercell that obeys the ice rules under periodic boundary conditions, using the combination of random shifting followed by the efficient chain propagation procedure described above. However, we still have the other problem of having to generate the Xe shielding response as a function of configuration in the Xe@XCAGE/PCA model in a form that could be used at an arbitrary Xe position in an arbitrary cage in a crystal fragment that has the space average crystallographic symmetry.

The water molecules in a given extended cage have a specific proton disorder. Cages with different proton configurations should give different shielding responses at the Xe nucleus. Comparing calculations based on unit cells with different proton configurations can reveal how large these differences are. In addition, in using one unit cell to propagate into a crystal fragment, we end up with a crystal fragment with the reinforced proton disorder of the original small unit. A point charge array with reinforced proton disorder will result in the water molecules of the cage having a different electronic structure than in a cage embedded in a point charge array that reflects the space average crystallographic symmetry.

TABLE IV. Average Xe shielding $\langle\sigma_{iso}\rangle - \sigma$(Xe atom), ppm, obtained using individual sets of 16 *ab initio* values obtained in the XCAGE/PCA model to generate individual shielding functions for Xe–O and Xe–H in each of three 5^{12} cages having different proton configurations.

Configuration	A	B	C
$\langle\sigma_{iso}\rangle - \sigma$(Xe atom)	−221.1	−210.8	−211.1

First, we show the magnitude of the differences between the calculated average Xe shieldings associated with particular proton configurations. In Table IV, we compare three such results. We have calculated 16 DFT/B3LYP shielding values (using the XCAGE/PCA model) for the 5^{12} cage in Structure I for Xe in various positions within the small cage, employing unit cells with proton configuration A, B, and C. Each set of 16 calculated values is fitted to Xe–O and Xe–H shielding response functions of the form shown in Eq. (1). Each surface was used to calculate a canonical Monte Carlo average shielding. We anticipated the results to differ, and in fact we find that using a specific proton configuration, both to generate the shielding surface and to perform the canonical Monte Carlo simulation, results in a particular average isotropic Xe shielding, slightly different from the shielding value arising from a different proton configuration. The values given in Table IV are the results from averaging over 10^6 system configurations.

To improve upon this, we need to randomly pick a cage within a large supercell and do the *ab initio* or DFT Xe shielding calculations at various locations in the cage, then do this for some number of cages and average the results. An average over a large number of such calculations, only three of which are represented in Table IV, would be prohibitive. The Monte Carlo averaging is inexpensive, but the quantum mechanical calculations and fitting the values to shielding functions are time consuming. Therefore, we choose the following approach. We use a small representative number of cages to carry out quantum mechanical calculations, to produce Xe–O and Xe–H shielding functions that can describe the Xe shielding response in any cage with any proton disorder. To obtain these universal shielding functions, we fit all of the quantum mechanically calculated points together to the same set of coefficients, so that the proton configurations are averaged together in the fitting. We then use this shielding surface as a universal shielding surface that applies to any cage in any point charge array. In principle, if we include enough proton configurations in the fitting, the universal shielding function will only be systematically inaccurate in the sense that in every cage the Xe is feeling a reinforced

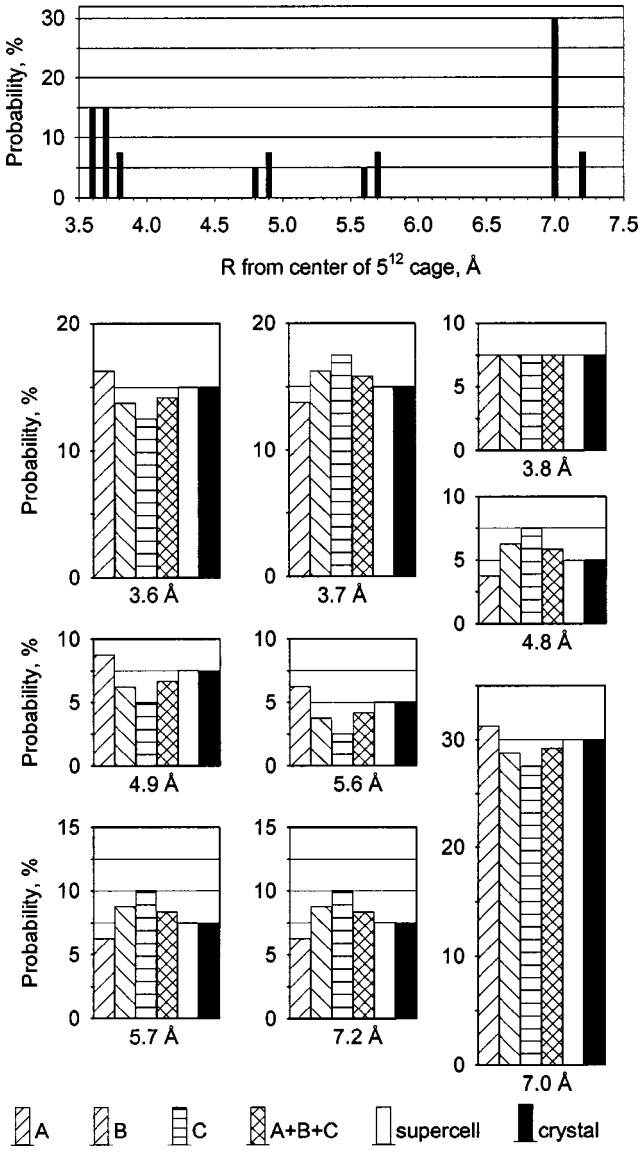

FIG. 4. The distributions of proton positions from the center of the 5^{12} cage in Structure I, including all hydrogen atoms within the extended cage. The models based on unit cells with proton configurations A, B, and C are compared with the distribution for the composite of A+B+C, for the supercell used as the simulation box for the averages reported in Table VI, and for the crystallographic data with 1/2 population at each proton position. All proton positions are based on the neutron diffraction data of Ref. 31 and in each case a crystal fragment with 4×4×4 unit cells is the basis for the calculated distributions.

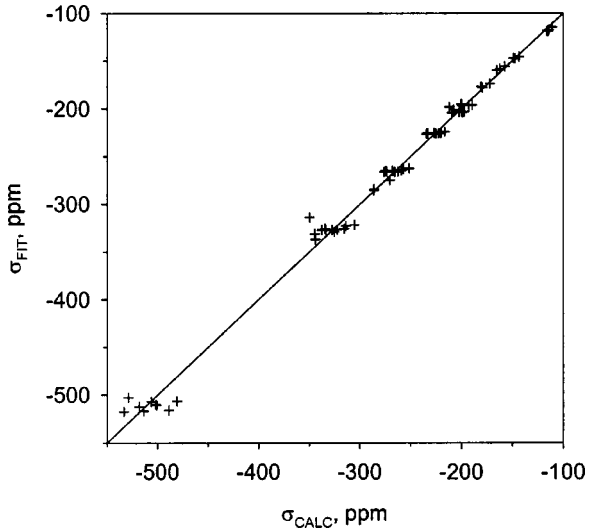

FIG. 5. The values regenerated by the fitted functions of Eq. (1), σ_{FIT}, are compared with the corresponding isotropic shielding values from quantum mechanical calculations (DFT/B3LYP), σ_{CALC}, for the same Xe positions. Only the calculations based on the XCAGE/PCA model are included here.

disordered environment, but many different reinforced disorders are represented.

The accuracy of the universal shielding function obtained by this procedure is determined by how closely the few unit cells together represent the crystallographic proton distribution. In order to test how well the three different proton disorders in unit cells A, B, and C reproduce the crystallographic symmetry, we compared the corresponding proton distributions. That is, we determined the number of protons located at a certain distance from the center of the small cage in the XCAGE/PCA models with proton configuration A, B, and C. The comparison is shown in Fig. 4. We find that the diversity in the proton disorder in the three cages in Table IV was sufficient, that, when combined together, they reproduce closely the distribution of proton distances in the supercell and the latter accurately reproduced the distribution in the crystal. We therefore fitted all the calculated shielding values for the three configurations together to arrive at a common shielding surface. Even better, we found that this combined shielding surface could reproduce the original shielding values for Xe in specific locations in the large $5^{12}6^2$ cage that were calculated independently. Thus, we combined all the calculated values together, and found a single set of Xe–O and Xe–H shielding response functions [i.e., the coefficients $a_6,\ldots,a_{12}$, $b_6,\ldots b_{12}$ in Eq. (1)] that described very well the entire set (73 points) of quantum mechanically calculated values. This is the universal shielding surface that we use for all the Monte Carlo simulations described below for the small and large cages in a supercell of clathrate hydrate Structure I, and for the small and large cages in a supercell of clathrate hydrate Structure II. The comparison of the quantum mechanical values against the fit to Eq. (1) is given in Fig. 5 and the Xe–O and Xe–H shielding response functions that are arrived at by the fitting procedure are shown in Fig. 6. At a given distance, the O atom provides a greater shielding response at the Xe nucleus than does the H atom.

Average isotropic Xe shielding

The universal shielding surface obtained above is used in canonical Monte Carlo simulations in a supercell simulation box, as described in the Methods section. The same shielding functions and the same potential functions are used in all simulations. In Fig. 7(a) we show the Xe shielding surface for Xe positions on a specific plane, the plane passing through the center of the $5^{12}6^2$ cage in clathrate hydrate Structure I. Figure 7(b) shows the one-body distribution function for the Xe in this plane at 275 K. The average shielding is the value of the isotropic shielding given by the shielding surface in Fig. 7(a) weighted by the probability of

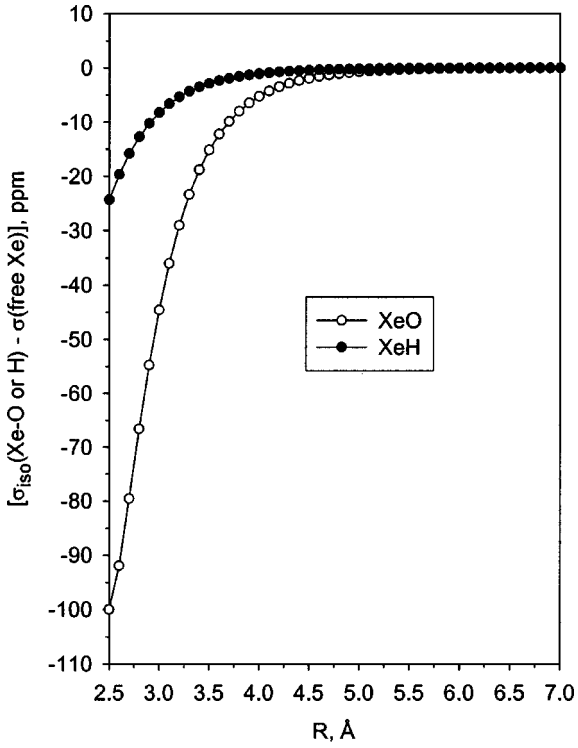

FIG. 6. The Xe–O and Xe–H universal isotropic shielding response functions that comprise the shielding surface described by Eq. (1) for Xe in clathrate hydrates.

finding the Xe at that position, given by the one-body distribution function shown in Fig. 7(b), with the sums carried out over all Xe positions. Of course, the mathematical surfaces shown in Figs. 7(a) and 7(b) illustrate only the values at a specific z coordinate (in the plane shown); the Monte Carlo procedure includes a large number of configurations representative of all coordinates for the Xe atom in three dimensions.

The precision and accuracy of the average isotropic Xe shielding will depend on the size of the supercell used as a simulation box and the total number of Xe configurations used in the Monte Carlo simulations. A larger simulation box provides a larger number of different proton configurations for the cages the Xe atom explores throughout the simulation. Increasing the number of Monte Carlo loops without changing the size of the simulation box improves the precision but not the accuracy of the averages obtained. We investigated the number of cages in the supercell required to obtain a statistically valid average in clathrate hydrate Structure I. A comparison in Table V of the averages obtained using different sizes of the simulation box demonstrates the convergence of the average Xe shielding values upon increasing the size of the supercell while keeping the total number of Xe configurations the same. Averaging in a simulation box of $6\times6\times6$ unit cells leads to an average shielding for a Xe atom in the 5^{12} cages in Structure I that does not significantly differ from the results obtained using $4\times4\times4$ or $2\times2\times2$ unit cells. We find that using a supercell of $2\times2\times2$ or $4\times4\times4$ unit cells as the simulation box is sufficient to obtain an average Xe shielding response that is statistically valid for the 5^{12} cages of Structure I.

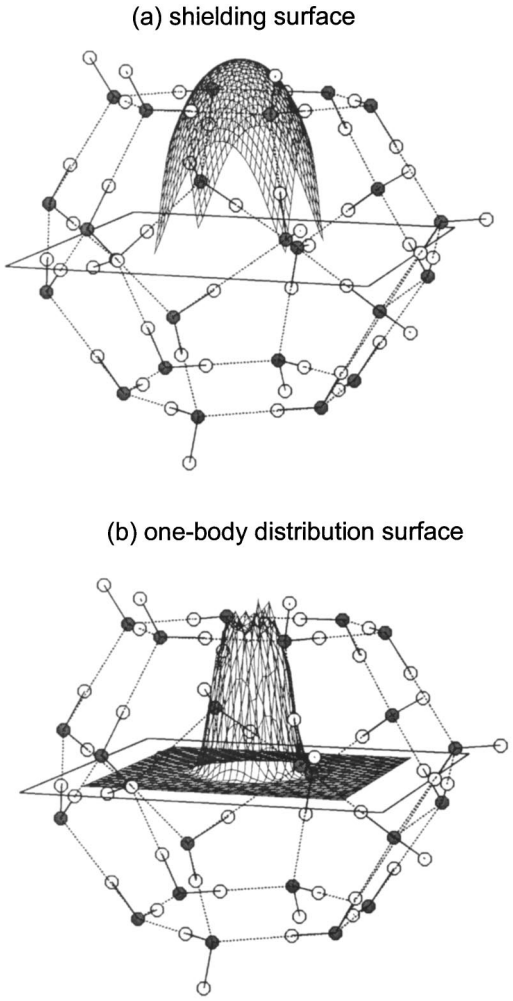

FIG. 7. (a) The isotropic shielding surface gives the magnitude of the shielding response at the Xe nucleus at various positions in the plane perpendicular to the unique axis and passing through the center of the $5^{12}6^2$ cage in clathrate hydrate Structure I. (b) The one-body distribution function shows the probability of finding the Xe atom at various positions in the same plane as in (a).

Finally, the average shieldings calculated for Xe in the small and large cages of Structure I and Structure II are shown in Table VI. In order to have comparable accuracy in the averages for the Xe shielding in the 5^{12} cages of Structure I and II, we show the results using a simulation box of $4\times4\times4$ unit cells for Structure I and $2\times2\times2$ unit cells for Structure II. The averages obtained here are in good agree-

TABLE V. Average isotropic shielding of Xe in the small cages of clathrate hydrate Structure I at 275 K in different sizes of simulation box, using the universal Xe–O and Xe–H shielding functions fitted to 73 *ab initio* shielding values.

Simulation box, unit cells	Number of 5^{12} cages	$\langle\sigma(\text{Xe@}5^{12})\rangle-\sigma(\text{free Xe atom})$, ppm
XCAGE config A, B, C	1	−214.905, −214.617, −214.500
1×1×1	2	−214.383
2×2×2	16	−214.065
4×4×4	128	−214.076
6×6×6	432	−214.038

TABLE VI. Average isotropic shielding of Xe, $\langle\sigma_{iso}\rangle - \sigma$(Xe atom), ppm, in the small and large cages of clathrate hydrate Structure I and Structure II. These were calculated at 275 K using the Xe–O and Xe–H universal shielding functions derived from 73 *ab initio* values.

	Number of cages in simulation box	Calculated $\langle\sigma_{iso}\rangle - \sigma$(Xe atom)	Experiment $\langle\sigma_{iso}\rangle - \sigma$(Xe atom)
Small (5^{12}) cage, I	128	−213.98	−242[a]
Large ($5^{12}6^2$) cage, I	384	−146.93	−152[a]
Small (5^{12}) cage, II	128	−206.7	−225[b,c]
Large ($5^{12}6^4$) cage, II	64	−104.67	−80[b,d]

[a]Reported at 263–293 K in Ref. 22, at 275 K in Ref. 23, and at 200–240 K in Ref. 24. At 77 K, a value of −250 and −148 ppm, for 5^{12} and $5^{12}6^2$, respectively, has been reported in Ref. 53. More precise measurements made possible by the use of hyperpolarized ^{129}Xe give −244.6 and −154.9 ppm, respectively, at an ambient temperature. (Ref. 29).

[b]Reported in the Xe-propane double hydrate at 200–240 K in Ref. 24 and in Xe-*n* butane double hydrate at 77 K in Ref. 27. Minor chemical shift differences (up to *ca.* 20 ppm) for the same resonance in different samples are reported in Ref. 27.

[c]With tetrahydrofuran or 1,1,1-dichlorofluoroethane in the $5^{12}6^4$ cage, Xe chemical shifts in the 5^{12} cage are somewhat larger, 234.2 and 231.8 ppm, respectively (Ref. 29).

[d]A value of −86 ppm has been reported at 77 K in Ref. 53.

ment with the trends in the experimental values; we reproduce the relative order of experimental ^{129}Xe chemical shifts in the four types of cages. We also achieve reasonably good agreement with the individual magnitudes of the chemical shifts relative to the free Xe atom, despite the approximations used here: the potential functions were not optimized to reproduce the Xe chemical shifts, nonpairwise additive terms in the intermolecular shielding response are neglected, and a finite number of cages are included in the supercell simulation box.

The differences between the cage structures are responsible for the differences found in the average isotropic Xe shieldings. In Fig. 1, the small (5^{12}) and large ($5^{12}6^2$) cages of Structure I clathrate hydrate are compared with the 5^{12} and $5^{12}6^4$ cages of Structure II. The different cage structures lead to different one-body distribution functions for the Xe atom (not shown). The universal Xe–O and Xe–H shielding functions are used for all cages. Since the shielding surface is less deshielded at larger Xe distances from the oxygen and hydrogen atoms, the larger the cage, the greater the fraction of Xe positions that make only small contributions to the overall deshielding. The distribution functions for Xe in the larger cages permit the Xe to be found at locations where the shielding response is weaker. Upon considering the differences between the cage structures shown in Fig. 1, the relative order of the average isotropic Xe shielding in the four types of cages is easily understood.

CONCLUSIONS

We have considered the average shielding for Xe in the small and large cages of clathrate hydrates Structures I and II. The Xe shielding response is shown to be very sensitive to the electronic structure of the close neighbors. We have shown that the electrostatic contributions to intermolecular shielding of a Xe atom are small and negligible. On the other hand, the electrostatic contributions from neighboring water molecules in the extended lattice to the electronic structure of the water molecules constituting a cage are not at all negligible, and this has a corresponding effect on the Xe shielding response to the water molecules of the cage. When the hydrogen bonding of the water molecules of the cage is incompletely described (such as when their hydrogen-bonding partners are either absent or represented merely by partial point charges, thereby leaving out the covalent part of the hydrogen bonding), these cage water molecules do not provide the correct shielding response at the Xe nucleus. It requires at least the first shell of additional water molecules to get a realistic description. By using the five models that incorporate some but not all of the electronic coupling of the Xe atom to the clathrate cages in the crystal, we have demonstrated which of the factors are important, and to what extent excluding them from the model compromises the description of Xe shielding in any hydrogen-bonded system. We provide a paradigm for the general treatment of intermolecular shielding in a hydrogen-bonded network. Universal Xe–O and Xe–H shielding functions are obtained by fitting together the quantum mechanical values calculated using the XCAGE/PCA model of several cages with diverse proton arrangements representing clathrate hydrate Structure I. Simulation boxes consisting of supercells are used with the same set of shielding functions and the same set of potential parameters to provide Monte Carlo averages of the isotropic Xe shielding in the small and large cages of clathrate hydrate Structures I and II. These average shieldings are in good agreement with the values observed by Ripmeester *et al.*[22–24,29] The results presented here are the first calculations of Xe shielding in clathrate hydrates and the first calculations of Xe shielding in a hydrogen-bonded system.

ACKNOWLEDGMENTS

This research was funded by the National Science Foundation (Grant No. CHE-9979259). We wish to thank Lewis Wedgewood for suggesting the hydrogen shifting technique.

[1] XEMAT 2000 Optical Polarization and Xenon NMR of Materials Proceedings, 28–30 June, 2000, Sestri Levante, Italy.
[2] J. L. Bonardet, J. Fraissard, A. Gedeon, and M. A. Springuel-Huet, Catal. Rev. - Sci. Eng. **41**, 115 (1999).

[3] C. I. Ratcliffe, *Annual Reports on NMR Spectroscopy*, edited by G. A. Webb (Academic, London, 1998), Vol. 36, pp. 123–221.
[4] B. M. Goodson, J. Magn. Reson. **155**, 157 (2002).
[5] P. Sozzani, A. Comotti, R. Simonutti, T. Meersman, J. W. Logan, and A. Pines, Angew. Chem., Int. Ed. Engl. **39**, 2695 (2000).
[6] T. R. Stengle and K. L. Williamson, Macromolecules **20**, 1428 (1987).
[7] J. B. Miller, Rubber Chem. Technol. **66**, 455 (1993).
[8] S. M. Rubin, S. Y. Lee, E. J. Ruiz, A. Pines, and D. E. Wemmer, J. Mol. Biol. **322**, 425 (2002).
[9] K. W. Miller, N. V. Reo, A. J. Uiterkamp, D. P. Stengle, T. R. Stengle, and K. L. Williamson, Proc. Natl. Acad. Sci. U.S.A. **78**, 4946 (1981).
[10] M. M. Spence, S. M. Rubin, I. E. Dimitrov, E. J. Ruiz, D. E. Wemmer, A. Pines, S. Q. Yao, F. Tian, and P. G. Schultz, Proc. Natl. Acad. Sci. U.S.A. **98**, 10654 (2001).
[11] C. J. Jameson and A. C. de Dios, J. Chem. Phys. **97**, 417 (1992).
[12] C. J. Jameson, D. N. Sears, and A. C. de Dios, J. Chem. Phys. **118**, 2575 (2003).
[13] C. J. Jameson, A. K. Jameson, B. I. Baello, and H. M. Lim, J. Chem. Phys. **100**, 5965 (1994).
[14] C. J. Jameson, A. K. Jameson, H. M. Lim, and B. I. Baello, J. Chem. Phys. **100**, 5977 (1994).
[15] C. J. Jameson, A. K. Jameson, and H. M. Lim, J. Chem. Phys. **104**, 1709 (1996).
[16] C. J. Jameson, A. K. Jameson, and H. M. Lim, J. Chem. Phys. **107**, 4364 (1997).
[17] C. J. Jameson, A. K. Jameson, P. Kostikin, and B. I. Baello, J. Chem. Phys. **112**, 323 (2000).
[18] C. J. Jameson, A. K. Jameson, R. E. Gerald II, and H. M. Lim, J. Phys. Chem. **101**, 8418 (1997).
[19] C. J. Jameson, J. Chem. Phys. **116**, 8912 (2002).
[20] C. J. Jameson and A. C. de Dios, J. Chem. Phys. **116**, 3805 (2002).
[21] C. J. Jameson and D. N. Sears, (unpublished).
[22] J. A. Ripmeester and D. W. Davidson, J. Mol. Struct. **75**, 67 (1981).
[23] D. W. Davidson, Y. P. Handa, and J. A. Ripmeester, J. Phys. Chem. **90**, 6549 (1986).
[24] J. A. Ripmeester, C. I. Ratcliffe, and J. S. Tse, Trans. Faraday Soc. **84**, 3731 (1988).
[25] J. A. Ripmeester, J. Am. Chem. Soc. **104**, 289 (1982).
[26] M. J. Collins, C. I. Ratcliffe, and J. A. Ripmeester, J. Phys. Chem. **94**, 157 (1990).
[27] J. A. Ripmeester and C. I. Ratcliffe, J. Phys. Chem. **94**, 8773 (1990).
[28] V. J. Storhaug, F. Liebig, and C. R. Bowers, J. Phys. Chem. B **106**, 2884 (2002).
[29] I. L. Moudrakovski, C. I. Ratcliffe, and J. A. Ripmeester, J. Am. Chem. Soc. **123**, 2066 (2001).
[30] I. L. Moudrakovski, A. A. Sanchez, C. I. Ratcliffe, and J. A. Ripmeester, J. Phys. Chem. B **105**, 12338 (2001).
[31] T. Ikeda, S. Mae, O. Yamamuro, T. Matsuo, S. Ikeda, and R. M. Ibberson, J. Phys. Chem. A **104**, 10623 (2000).
[32] R. K. McMullan and Å. Kvick, Acta Crystallogr., Sect. B: Struct. Sci. **46**, 390 (1990).
[33] L. J. Pauling, J. Am. Chem. Soc. **57**, 2680 (1935).
[34] J. D. Bernal and R. H. Fowler, J. Chem. Phys. **1**, 515 (1933).
[35] D. Stueber, F. N. Guenneau, and D. M. Grant, J. Chem. Phys. **114**, 9236 (2001).
[36] M. J. Frisch, G. W. Trucks, H. B. Schlegel *et al.*, GAUSSIAN 98, Revision A.9, Gaussian, Inc., Pittsburgh, PA, 1998.
[37] K. Wolinski, J. F. Hinton, and P. Pulay, J. Am. Chem. Soc. **112**, 8251 (1990).
[38] H. Partridge and K. Faegri, Jr., NASA Tech. Memo. 103918, 1992.
[39] D. M. Bishop and S. M. Cybulski, Chem. Phys. Lett. **211**, 255 (1993).
[40] S. F. Boys and F. Bernardi, Mol. Phys. **19**, 538 (1970).
[41] T. H. Dunning, Jr. and P. J. Hay, in *Modern Theoretical Chemistry*, edited by H. F. Schafer III (Plenum, New York, 1976), Vol. 3, p. 1.
[42] F. Lee, E. Gabe, J. S. Tse, and J. A. Ripmeester, J. Am. Chem. Soc. **110**, 6014 (1988).
[43] G. C. Maitland, M. Rigby, E. B. Smith, and W. A. Wakeham, *Intermolecular Forces, Their Origin and Determination* (Clarendon, Oxford, 1981).
[44] M. P. Allen and D. J. Tildesley, *Computer Simulations of Liquids* (Clarendon, Oxford, 1987).
[45] J. Gauss and J. F. Stanton, J. Chem. Phys. **104**, 2574 (1996).
[46] D. Stueber and D. M. Grant, J. Am. Chem. Soc. **124**, 10539 (2002).
[47] D. Stueber and D. M. Grant, Solid State Nucl. Magn. Reson. **22**, 439 (2002).
[48] J. Hinton, P. Guthrie, P. Pulay, and K. Wolinski, J. Am. Chem. Soc. **114**, 1604 (1992).
[49] S. Dong, R. Ida, and G. Wu, J. Phys. Chem. **104**, 11194 (2000).
[50] J. A. Ripmeester, C. I. Ratcliffe, D. D. Klug, and J. S. Tse, Ann. N.Y. Acad. Sci. **715**, 161 (1994).
[51] F. Mauri, A. Pasquarello, B. G. Pfrommer, Y. G. Yoon, and S. G. Louie, Phys. Rev. B **62**, R4786 (2000).
[52] B. G. Pfrommer, F. Mauri, and S. G. Louie, J. Am. Chem. Soc. **122**, 123 (2000).
[53] K. A. Udachin, G. D. Enright, C. I. Ratcliffe, and J. A. Ripmeester, J. Am. Chem. Soc. **119**, 11481 (1997).